Zurich, Switzerland, September 12, 2006

CONCRETE MEMBERS WITH PLATE REINFORCEMENT: MECHANICAL BOND ANALYSIS

Tomaž Ulaga

Walt + Galmarini AG
Englischviertelstrasse 24
8032 Zurich, Switzerland

phone: +41–43-222 66 30
fax: +41-43-222 66 67
e-mail: tomaz.ulaga@galmarini.ch

Tomaž Ulaga is a consulting engineer at Walt + Galmarini AG in Zurich, Switzerland. His research at the Swiss Federal Institute of Technology (ETH) in Zurich, leading to a Dr. sc. techn. degree in 2003, has focused on the behaviour of concrete members with internal bar and external plate reinforcement.

Thomas Vogel

Institute of Structural Engineering (IBK)
ETH Zurich
8093 Zurich, Switzerland

phone: +41–1-633 31 34
fax: +41-1-633 10 64
e-mail: vogel@ibk.baug.ethz.ch

Thomas Vogel is professor of structural engineering at the Swiss Federal Institute of Technology (ETH) in Zurich. He is active in research, consulting and teaching in the areas of design, construction and maintenance of concrete structures.

Number of words: 3472 (from section ABSTRACT to section CONCLUSIONS)

Number of tables: 0

Number of figures: 13

NOTATION

a	coefficient
a_F	Fuller distribution function
d	aggregate particle diameter
d_s	column diameter
d_2, d_{02}	arbitrary, particular intersection circle diameter
d_3, d_{03}	arbitrary, particular aggregate particle diameter
c	aggregate embedment depth
d_{min}, d_{max}	minimum, maximum aggregate particle diameter
F	force
F_{mr}, F_{mt}	components of an aggregate particle interlocking force
F_{mx}, F_{mz}	components of an aggregate particle interlocking force
F_{Rv}	punching resistance force
G_g	shear modulus of the adhesive layer
f_c, f_{cw}	concrete cylinder compressive strength, concrete cube compressive strength
f_{ct}, $f_{c\tau}$	concrete tensile strength, concrete shear strength
G_g	adhesive shear modulus
h	depth of a flat slab
K	aggregate particle
M	bending moment
M_{my}	interlocking moment of an aggregate particle
M_{DK}	punching cone surface
N_l	normal force in the plate reinforcement
n	probability density of the number of intersection circles
P	probability; point
p	probability density
q	distributed load
s_k	contact length
s_l	slip of the plate reinforcement
s_{l0}, s_{l1}	characteristic bond model slip values
s_1	line segment with unit length
$\bar{s}$	secant with average length
t	depth of a crack plane
t_g	thickness of the adhesive layer
u	horizontal component of v
u_0	horizontal component of v_0
V	shear force
V_c, V_k	volume of a concrete body, of the entire amount of aggregate particles
V_{kal}, V_{tot}	volume of an aggregate sphere cap, of an aggregate sphere
v	length of a crack opening vector
v_0	particular length of a crack opening vector
v_{min}, v_{max}	minimum, maximum length of a crack opening vector
w	vertical component of v (crack width)
w_0	vertical component of v_0 (particular value of crack width)

x	coordinate
y	coordinate
z	coordinate
γ_g	shear deformation of the adhesive layer
γ_g	ultimate shear deformation of the adhesive layer
μ	coefficient of friction
ρ_k	aggregate ratio
σ_c	normal stress in the concrete body
σ_{mus}	normal stress between an aggregate particle and the cement matrix
σ_v	interlocking normal stress
τ_c, τ_g	shear stress in the concrete body, in the adhesive layer
τ_{gu}	shear strength of the adhesive layer
τ_{mu}	shear stress between an aggregate particle and the cement matrix
τ_{l0}	bond shear strength of the plate reinforcement
τ_v	interlocking shear stress
φ	half contact angle
$\overline{\varphi}$	average half contact angle
ψ	polar coordinate

ABSTRACT

The bond stresses between a concrete body and plate reinforcement are often modelled with a bilinear bond stress-slip relationship. The mechanisms that govern this approach can be investigated on a micro-mechanical level in order to obtain a scientific model basis. As long as the load level is "low" the theory of elasticity can be used. When the load level is "high" a crack plane in the concrete body separates the constituents. Due to aggregate interlock mechanisms bond stresses still exist. This process can be investigated with the *Model of the Inclined Crack Opening, MICO*. The combination of the cases "bond at low load" and "bond at high load" provides a stress-slip diagram which is very similar to the bilinear bond model.

The *MICO* also has the potential to be used for the analysis of shear failure modes in concrete structures. The punching of a flat slab can be considered to show the possibilities.

INTRODUCTION

The application of externally bonded steel plates for the strengthening of reinforced concrete structures was already widespread in the 1970s. In the 80s and 90s research projects aimed at establishing the use of carbon fibre-reinforced plastic (CFRP) laminates for the same purpose [1]. Since then, this strengthening method has been used even more often and today many applications can be found.

The interaction between the components concrete and plate reinforcement requires the presence of bond stresses which enable the transfer of forces. In most practical cases, the existence of this basis is considered as given and no further investigations are performed. In fact, there are only a few scientifically established and applicable approaches which are suited to treat such questions.

The bilinear bond stress-slip relationship appears to be the most powerful existing analysis tool. It was applied to derive very useful anchorage capacity formulas [2] and to model concrete tension chords with internal bar and external plate reinforcement [3]. Despite these successes, the mechanical background of this bond model has not been investigated yet.

This paper presents the *Model of the Inclined Crack Opening*, *MICO*. The model is based on aggregate interlock mechanisms which can be found in a multitude of concrete structure failure modes, e.g. the debonding of plate reinforcement or the punching of flat slabs. Hence, the *MICO* represents a new tool which can be used for scientific structural analysis purposes.

THE BILINEAR STRESS-SLIP BOND MODEL

Significance

In Fig. 1(a) the principle of an anchorage capacity test is illustrated. This type of experiment has often been used for the investigation of the bond between a concrete body and plate reinforcement [2, 4, 5, 6]. The results provided new findings about the subject of interest.

In order to find explanations for the experimental observations the bond mechanisms were also investigated theoretically. In many cases a displacement-based bond theory was used for the modelling task [2, 3, 4, 5]. This method assumes a relationship between the relative displacement of the

concrete body and the plate reinforcement (slip) and the appropriate bond stresses. The form of this relationship is of major importance: a simple curve enables analytical treatment of the theory while a more complicated one appears to represent a more accurate approach to reality.

In recent publications [2, 3, 4, 5, 7] a bilinear bond stress-slip relationship according to Fig. 1(b) has been successfully used for theoretical bond investigations. With this tool, some very simple but powerful anchorage capacity formulas were derived [2, 3, 7, 8]. The bilinear bond stress-slip relationship was also used for the analysis of tension chords with internal bar und external plate reinforcement [3], Fig. 1(c). Both applications provided results which display a very good agreement with experimental data.

Quantification

The vertices of the bilinear bond stress-slip relationship in Fig. 1(b) must be quantified in order to derive numerical results from the theoretical model. Experimental data from a multitude of authors can be considered in order to find appropriate values [2, 4, 5, 6]. The recommendations in Eq. (1)…(3) originate from calibration work with tests that basically correspond to the anchorage capacity test in Fig. 1(a). It has been shown that these values also provide excellent results for modelling tasks outside the range of the calibration data [3].

$$\tau_{l0} = 0.4 \cdot f_c^{2/3} \tag{1}$$

$$s_{l0} = \frac{G_g}{t_g} \cdot \tau_{l0} \tag{2}$$

$$s_{l1} = s_{l0} + 0.225[mm] \tag{3}$$

THEORY OF BOND MECHANISMS

Overview

In Fig. 2(a) a reinforced concrete beam strengthened with external plate reinforcement is shown. The subject of interest is the bond between the plate reinforcement and the concrete surface. The detail in Fig. 2(b) displays a longitudinal section through the interface region in the unloaded state of the beam. This scheme can be used for some micro-mechanical bond investigations.

"Bond at low load"

Basics

Fig. 3(a) shows a plate-concrete bond situation "at low load". A relative displacement, *u*, between the concrete body and the plate reinforcement is possible due to shear deformation of the adhesive layer.

Assumptions

The shear deformations are considered to be concentrated in the adhesive layer only. The corresponding shear stress-shear strain relationship is given in Fig. 3(b). A continuous increase of the load will lead to the sudden development of a crack in the weakest element, i.e. in the concrete body. When this occurs the bond situation becomes that of "bond at high load".

Modelling

With the diagram in Fig. 3(b) the deformation can be determined according to Eq. (4). A crack in the concrete body will start to grow when the shear stress τ_{l0} is reached. This stress is related to the concrete shear strength, $f_{c\tau}$, which can be estimated with the modified Coulomb failure criterion [9] in Fig. 3(c). In fact, τ_{l0} exceeds this value, because it is the strength parameter at one particular position, while $f_{c\tau}$ indicates the strength of the weakest location of an entire structural member. Hence, Eq. (5) can be used to estimate the value of τ_{l0}.

$$s_l = \frac{t_g}{G_g} \cdot \tau_l \tag{4}$$

$$\tau_{l0} = a \cdot f_{c\tau} = a \cdot f_{ct} \qquad a \geq 1.0,\ f_{ct} = 0.3 \cdot f_c^{2/3} \tag{5}$$

"Bond at high load"

Basics

The detail in Fig. 4(a) displays the bond mechanisms "at high load", where a crack plane has separated the plate from the concrete body. Apparently, the increase of the horizontal displacement, u, also requires an increase of the crack width, w. In order to model the geometry of this process a simple assumption appears to be appropriate: the displacement of the faces of the crack is governed by an inclined opening where the angle α is the decisive parameter. For compatibility reasons the aggregate particles cause local abrasion effects in the matrix of the opposite crack face. This aggregate interlock mechanism enables the transfer of bond forces across the crack plane.

The analysis of aggregate interlock mechanisms was investigated by Walraven [10, 11]. He established a closed-form mathematical model which he used to determine bond stresses in specimens which were subjected to pure shear load. In the case of the present considerations the displacement process is different, so that Walraven's theory must be modified in order to build up the *Model of the Inclined Crack Opening, MICO*.

Assumptions

The concrete body consists of perfectly rigid and spherical aggregate particles which are embedded in a cement matrix. The aggregate ratio, ρ_k, is defined according to Eq. (6) and the distribution of the diameters is described by the Fuller function, Eq. (7).

$$\rho_k = \frac{V_k}{V_c} \tag{6}$$

$$a_F(d) = \sqrt{\frac{d}{d_{\max}}} \tag{7}$$

The abrasion of the matrix causes normal and shear stresses, σ_{mu} and τ_{mu}, in the aggregate-cement contact zone, Figure 4(c). σ_{mu} is a perfectly plastic (and therefore constant) strength parameter, τ_{mu} is the corresponding frictional stress, Eq. (8).

$$\tau_{mu} = \mu \cdot \sigma_{mu} \tag{8}$$

Modelling

1. Probabilistic aspects

The geometry of a crack surface is complex and cannot be modelled with simple explicit formulas. Due to the variation of the sizes, of the distances and of the embedment depths of the aggregate particles the use of probabilistic methods becomes necessary. The question that will be treated in this section is how many sphere caps can be expected to be found in a unit area of a crack face.

Firstly, the three-dimensional concrete structure will be considered. d_{03} is the diameter of a particular aggregate particle. Eq. (6) and (7) can be used to determine the probability that an arbitrary point in the concrete structure is located in an aggregate particle which has a diameter d_3 that is smaller than d_{03}, Eq. (9). Differentiation of this function leads to the corresponding probability density function, Eq. (10).

$$P[K \cap (d_3 < d_{03})] = \rho_k \cdot \sqrt{\frac{d_{03}}{d_{\max}}} \tag{9}$$

$$p[K \cap (d_3 = d_{03})] = \frac{\partial}{\partial d_{03}} P[K \cap (d_3 < d_{03})] = \frac{\rho_k}{2 \cdot \sqrt{d_{\max} \cdot d_{03}}} \tag{10}$$

The intersection circle of the aggregate particle and the plane in Fig. 5(a) has the diameter d_{02}. The probability that an arbitrary point in this particle is located in an intersection circle which has a diameter which is smaller than d_{02} can be calculated according to Eq. (11).

$$P[d_2 < d_{02}] = \frac{2 \cdot V_{kal}}{V_{tot}} = 1 - \left[1 + \frac{1}{2} \cdot \left(\frac{d_{02}}{d_{03}}\right)^2\right] \cdot \sqrt{1 + \left(\frac{d_{02}}{d_{03}}\right)^2} \tag{11}$$

The probability that an arbitrary point of a plane is located in an aggregate particle and the corresponding intersection circle has a diameter which is smaller than d_{02} can now be determined. If the point is located in an aggregate particle with $d_3<d_{02}$, Eq. (11) becomes irrelevant. Hence, the solution according to Eq. (12) consists of two terms which correspond to the cases $d_3<d_{02}$ and $d_3 \geq d_{02}$, respectively. Differentiation of Eq. (12) results in the probability density function according to Eq. (13).

$$\begin{aligned} P[K \cap (d_2 < d_{02})] &= \int_{d_3=0}^{d_3=d_{02}} p[K \cap (d_3 = d_{03})] \partial d_3 + \int_{d_3=d_{02}}^{d_3=d_{\max}} p[K \cap (d_3 = d_{03})] \cdot P[d_2 < d_{02}] \partial d_3 \\ &= \rho_k - \int_{d_3=d_{02}}^{d_3=d_{\max}} \left\{ \left[1 + \frac{1}{2} \cdot \left(\frac{d_{02}}{d_{03}}\right)^2\right] \cdot \sqrt{1 + \left(\frac{d_{02}}{d_{03}}\right)^2} \cdot \frac{\rho_k}{2 \cdot \sqrt{d_{\max} \cdot d_3}} \right\} \partial d_3 \end{aligned} \tag{12}$$

$$\begin{aligned} p[K \cap (d_2 = d_{02})] &= \frac{\partial}{\partial d_{02}} P[K \cap (d_2 < d_{02})] \\ &= \frac{\partial}{\partial d_{02}} \left\{ \rho_k - \int_{d_3=d_{02}}^{d_3=d_{\max}} \left\{ \left[1 + \frac{1}{2} \cdot \left(\frac{d_{02}}{d_{03}}\right)^2\right] \cdot \sqrt{1 + \left(\frac{d_{02}}{d_{03}}\right)^2} \cdot \frac{\rho_k}{2 \cdot \sqrt{d_{\max} \cdot d_3}} \right\} \partial d_3 \right\} \end{aligned} \tag{13}$$

A line segment, s_1, which has the length 1 contains all points which lie on the direct connection of the two ends. Hence, the part of this line which is located in aggregate intersection circles with $d_2=d_{02}$ can be determined according to Eq. (14).

$$p[s_1 \cap K \cap (d_2 = d_{02})] = 1 \cdot p[K \cap (d_2 = d_{02})] \tag{14}$$

In Fig. 5(b) an aggregate intersection circle and a rectangle of equal height and area are given. Hence, the width of the rectangle according to Eq. (15) corresponds to the average length of an intersection circle secant, $\bar{s}$.

The present section aims at treating the question of how many sphere caps can be expected in a unit area of a crack face. The answer can be formulated as a probability density function for the two-dimensional case: Eq. (16) indicates the number of intersection circles with a diameter d_{02} which can be expected to be intersected by a horizontal line segment of length 1.

$$\bar{s} = \frac{d_{02} \cdot \pi}{4} \tag{15}$$

$$n[s_1 \cap K \cap (d_2 = d_{02})] = \frac{p[s_1 \cap K \cap (d_2 = d_{02})]}{\bar{s}} = \frac{4 \cdot p[K \cap (d_2 = d_{02})]}{d_{02} \cdot \pi} \tag{16}$$

2. Consideration of a single aggregate intersection circle

The intersection circle in Fig. 6 has an embedment depth, c, which is greater or equal to 0 (otherwise the aggregate particle is located in the opposite crack face). The crack opening vector, v, can vary between a minimum value (where the crack is closed) and a maximum value (where the contact between the aggregate particle and the opposite crack face disappears). The characteristic values of v and the corresponding contact length, s_k, can be found by considering Fig. 6, Eq. (17)…(20):

- The crack is closed, Fig. 6(a)

$$v = v_{\min} = 0 \tag{17}$$

- General case, Fig. 6(b)

$$v = v_0 = [v_{\min} \ldots v_{\max}] \tag{18}$$

$$\sin(2\varphi) = \sqrt{1 - \left(2 \cdot \frac{w_0 + c}{d_{02}}\right)^2} \cdot \cos\alpha - \left(2 \cdot \frac{w_0 + c}{d_{02}}\right) \cdot \sin\alpha \tag{19}$$

$$s_k = d_{02} \cdot \varphi \tag{20}$$

- Contact length reduced to a point, Fig. 6(c)

$$v = v_{\max} = \left(\frac{d_{02}}{2} \cdot \cos\alpha - c\right) \cdot \frac{1}{\sin\alpha} \tag{21}$$

$$\varphi = 0\,,\ s_k = 0 \tag{22}$$

The general case according to Fig. 6(b) can be considered to determine the interlocking force of a single aggregate particle, Fig. 7. The contact stresses, σ_{mu} and τ_{mu}, can be replaced by the resulting force at the centre of the intersection circle or its orthogonal components, Eq. (23)…(26), respectively. The moment, M_{my}, does not need to be considered, because each crack face has the same number of protruding aggregate spheres as deepened aggregate holes. The appropriate moments have opposite signs and therefore the resulting moment is equal to zero.

$$F_{mr}(\varphi) = \int_{-\varphi}^{\varphi} \frac{d_{02}}{2} \cdot \cos\psi \cdot \sigma_{mu}\, \partial\psi + \int_{-\varphi}^{\varphi} \frac{d_{02}}{2} \cdot \sin\psi \cdot \tau_{mu}\, \partial\psi = d_{02} \cdot \sigma_{mu} \cdot \sin\varphi \tag{23}$$

$$F_{mt}(\varphi) = \int_{-\varphi}^{\varphi} \frac{d_{02}}{2} \cdot \cos\psi \cdot \tau_{mu}\, \partial\psi + \int_{-\varphi}^{\varphi} \frac{d_{02}}{2} \cdot \sin\psi \cdot \sigma_{mu}\, \partial\psi = d_{02} \cdot \tau_{mu} \cdot \sin\varphi \tag{24}$$

$$F_{mx}(\varphi) = F_{mr} \cdot \sin(\alpha + \varphi) + F_{mt} \cdot \cos(\alpha + \varphi) = d_{02} \cdot \sigma_{mu} \cdot \sin\varphi \cdot [\sin(\alpha + \varphi) + \mu \cdot \cos(\alpha + \varphi)] \tag{25}$$

$$F_{mz}(\varphi) = F_{mr} \cdot \cos(\alpha + \varphi) - F_{mt} \cdot \sin(\alpha + \varphi) = d_{02} \cdot \sigma_{mu} \cdot \sin\varphi \cdot [\cos(\alpha + \varphi) - \mu \cdot \sin(\alpha + \varphi)] \tag{26}$$

3. Boundary conditions

Normally, the crack plane is located in the vicinity of the concrete surface. This region is influenced by a lack of big aggregate particles because the formwork has pushed them towards the core of the concrete body. The corresponding sphere caps have a limited height which leads to a reduction of the interlocking contribution.

The coherence between the depth of the crack plane, t, and the embedment depth of the aggregate particles, c, can be investigated according to Fig. 8. This consideration provides the boundary conditions which are given in Eq. (27)…(29):

- "Small" aggregate particle in the concrete surface region, Fig. 8(a)

$$c_{\min} = 0 \tag{27}$$

- "Big" aggregate particle in the concrete surface region, Fig. 8(b)

$$c_{\min} = \frac{d_{02}}{2} - t \tag{28}$$

- "Big" embedment depth, no interlocking contribution, Fig. 8(c)

$$c_{\max} = \frac{d_{02}}{2} \cdot \cos\alpha \tag{29}$$

Generally, the range of the embedment depth is $c = [0 \ldots d_{02}/2]$. If all values of c have the same incidence, the probability density function for a particular value can be determined according to Eq. (30).

$$p[c] = \frac{2}{d_{02}} \tag{30}$$

The expected value of the average (half) contact angle of an aggregate intersection circle, $\bar{\varphi}$, can now be estimated. For this purpose, the product of $p[c]$, Eq. (30), and φ, Eq. (19), must be integrated over the range of all possible embedment depths. Individual treatment of the cases "small" and "big" aggregate particle leads to Eq. (31) and (32), respectively.

$$d_{02} < 2 \cdot t: \qquad \bar{\varphi}_{<2t}(d_{02}) = \int_{c_{\min}}^{c_{\max}} p[c] \cdot \varphi \, \partial c = \frac{2}{d_{02}} \cdot \int_{0}^{\frac{d_{02}}{2}\cdot\cos\alpha} \varphi \, \partial c \tag{31}$$

$$d_{02} > 2 \cdot t: \qquad \bar{\varphi}_{>2t}(d_{02}) = \int_{c_{\min}}^{c_{\max}} p[c] \cdot \varphi \, \partial c = \frac{2}{d_{02}} \cdot \int_{\frac{d_{02}}{2}-t}^{\frac{d_{02}}{2}\cos\alpha} \varphi \, \partial c \tag{32}$$

4. Global interlocking stresses

The model elements which were derived in the previous sections can be combined in order to obtain the global interlocking stresses in Fig. 9, σ_v and τ_v. Generally, an aggregate intersection circle of diameter d_{02} was considered. Therefore, the factor "1" in Eq. (33) and (34) indicates the expansion from the two-dimensional case to the three-dimensional case. The argument of the integral consists of two factors: the number of aggregate intersection circles according to Eq. (16) and the average contact force per intersection circle according to Eq. (25), (26), (31) and (32). Finally, the integration from d_{min} to d_{max} provides a result which considers the entire range of all intersection circle diameters.

Eq. (33) and (34) represent the final results of the *MICO*. The evaluation of the expressions requires numerical procedures and therefore no further analytical treatment will be performed.

$$\sigma_v = 1 \cdot \int_{d_{\min}}^{d_{\max}} n[s_1 \cap K \cap (d_2 = d_{02})] \cdot F_{mz}(\bar{\varphi})\, \partial d_{02}$$
$$= 1 \cdot \left\{ \int_{d_{\min}}^{2 \cdot t} n[s_1 \cap K \cap (d_2 = d_{02})] \cdot F_{mz}(\bar{\varphi}_{<2t}(d_{02}))\, \partial d_{02} + \int_{2 \cdot t}^{d_{\max}} n[s_1 \cap K \cap (d_2 = d_{02})] \cdot F_{mz}(\bar{\varphi}_{>2t}(d_{02}))\, \partial d_{02} \right\} \quad (33)$$

$$\tau_v = 1 \cdot \int_{d_{\min}}^{d_{\max}} n[s_1 \cap K \cap (d_2 = d_{02})] \cdot F_{mx}(\bar{\varphi})\, \partial d_{02}$$
$$= 1 \cdot \left\{ \int_{d_{\min}}^{2 \cdot t} n[s_1 \cap K \cap (d_2 = d_{02})] \cdot F_{mx}(\bar{\varphi}_{<2t}(d_{02}))\, \partial d_{02} + \int_{2 \cdot t}^{d_{\max}} n[s_1 \cap K \cap (d_2 = d_{02})] \cdot F_{mx}(\bar{\varphi}_{>2t}(d_{02}))\, \partial d_{02} \right\} \quad (34)$$

Numerical examples

Parameters

The evaluation of the *MICO* requires a set of input data. The parameters can be subdivided into three different types: geometric parameters (which characterize the architecture of the concrete structure and the location of the crack plane), material parameters (for the quantification of the properties of the cement matrix) and kinematic parameters (which provide information about the crack opening process). For every single parameter a range of values can be indicated:

- The aggregate ratio, ρ_k, is defined according to Eq. (3). For normal concrete the values are in the range [12] $\rho_k = [0.70 \ldots 0.75]$.
- According to the CEB-FIB Model Code 1990 [13], the most common values for the maximum aggregate size are $d_{max} = [8, 16, 32]$ mm.
- The depth of the crack plane, t, follows from experimental experience with plate reinforced concrete structures. In many cases failure occurs due to debonding of the plate. The average thickness of the concrete layer which remains on the plate is equal to the depth of the crack plane. Several authors [5, 14] have observed that this value is in the range of $t = [1 \ldots 3]$ mm.
- The correlation between the concrete cube compressive strength, f_{cw}, and the strength parameter of the cement matrix, σ_{mu}, was investigated by Walraven [10, 11]. He used experimental data to calibrate the relationship in Eq. (32). In order to correlate this expression with the more often used concrete cylinder strength, f_c, substitution according to Eq. (33) is possible.
  $$\sigma_{mu} = 6.39 \cdot f_{cw}^{0.56} \quad (32)$$
  $$f_c = 0.8 \cdot f_{cw} \quad (33)$$
- Walraven also used his tests to find an appropriate value for the coefficient of friction, μ. His model provided good results with the approach according to Eq. (34).
  $$\mu = 0.4 \quad (34)$$
- According to the model assumptions, the crack opening angle, α, has a constant value. An accurate definition of α turns out to be difficult. The inclination of the principal stresses (which result from the shear stresses in and the normal stresses on the interface) indicates the "favourite opening angle" of the system. The rigid aggregate particles generally block that direction and therefore cause an opening that can not easily be described with a theoretical approach. Neubauer [4] carried out tests where he measured the horizontal and the vertical displacement of the plate reinforcement of concrete members. Evaluation of the data

leads to a range of $\alpha = [15° \ldots 65°]$. Hence, this empirical result can be used for the first model evaluations.

- The length of the crack opening vector, v, will be considered as a variable parameter. Hence, the relationship between the interlocking stresses and the crack opening displacement can be investigated. This parameter can also be divided into its components u (which is parallel to the crack plane) and w (which is normal to the crack plane).

Results

For a set of parameter combinations the results of the *MICO* are given in Fig. (10). The x-axis contains the crack opening parameters v, u and w, respectively. The interlocking stresses referring to the matrix strength and the aggregate ratio, $\tau_v/(\sigma_{mu} \cdot \rho_k)$ and $\sigma_v/(\sigma_{mu} \cdot \rho_k)$, are given on the y-axis.

Discussion

Consider the variation of the $\tau_v/(\sigma_{mu} \cdot \rho_k)$ –diagrams in Fig. 10. τ_v can be interpreted as bond shear stress between the concrete body and the plate reinforcement. Hence, these lines basically characterize the same process as the descending branch of the bilinear bond stress-slip relationship. The similarity appears to be amazingly good. Apparently, following parameters have a major influence on the magnitude of the bond stresses:

- A low value of the crack opening angle, α, leads to high bond stresses. In the case of real structures the crack opening angle can be reduced with compressive stresses on the plate reinforcement.
- A high value of the depth of crack plane, t, provides high bond stresses. Therefore, the concrete surface should be sufficiently roughened prior to the application of the plate reinforcement.
- A small value of the maximum aggregate size, d_{max}, leads to high bond stresses.

Modelling of the bilinear bond stress-slip relationship

The models of the cases "bond at low load" and "bond at high load" can be combined in order to derive a complete shear stress-slip diagram. The diagrams in Fig. 11 display the results of such a combination for a particular set of parameters. Simplification of the descending branch leads to a linear relationship. Hence, a scientific background for the bilinear bond stress-slip model has been established. In Fig. 11 the results of the two approaches are displayed.

AGGREGATE INTERLOCK MECHANISMS IN SHEAR CRACK OPENING

The failure mode of concrete structures which are subjected to shear load often corresponds to the mechanism of the inclined crack opening. Therefore, the *MICO* has the potential to be used for the analysis of such cases. An example will be considered in order to explain the procedure.

In Fig. 12(a) a punching situation is displayed. A detail of the cone-shaped punching body is displayed in Fig. 12(b). Apparently, the dislocation of the column and the flat slab results in an inclined crack opening. The corresponding interlocking stresses are displayed in Fig. 12(c). These stresses cause a punching resistance, F_{Rv}, which can be determined according to Eq. (35). The sur-

face of the punching cone follows from Eq. (36), the interlocking stresses, σ_v and τ_v, can be estimated with the *MICO*.

$$F_{Rv} = M_{DK} \cdot (|\tau_v| \cdot \cos\alpha - |\sigma_v| \cdot \sin\alpha) \tag{35}$$

$$M_{DK} = \pi \cdot \frac{h}{\cos\alpha} \cdot (h \cdot \tan\alpha + d_s) \tag{36}$$

The results of a numerical example are given in Fig. 13. The values of the parameters f_c, ρ_k, α, d_s, h are arbitrary but reasonable numbers to display the potential of the model .When the crack is still closed, the punching resistance has its maximum value which is independent of the maximum aggregate size, d_{max}. The opening of the crack then causes a steep drop of F_{Rv}.

The shear failure of a reinforced concrete beam or the pull-out resistance of an anchor could probably also be treated with the *MICO*. The present example does not consider the effect of internal bar reinforcement or the influence of flexural deformations. Therefore, several questions remain unanswered. Nevertheless the *MICO* appears to have considerable potential for the theoretical analysis of shear failure problems. Further research is necessary to figure out all the possibilities.

CONCLUSIONS

The relative displacement of a concrete body and plate reinforcement causes bond stresses in the interface. Simple assumptions can be used to estimate these stresses. In the case "bond at low load" relative displacement is possible due to shear deformations in the adhesive layer. Hence, the principles of the theory of elasticity can be applied. In the case "bond at high load" a crack plane separates the constituents. The relative displacement has a component which is parallel to the interface and one which is perpendicular to it. In order to investigate this process, the *Model of the Inclined Crack Opening*, *MICO*, can be used. The evaluation of these two cases provides a bond stress-slip relationship which can be idealized with a bilinear approach. Hence, a scientific background for the frequently used bilinear stress-slip relationship has been established.

The *MICO* can also be used to determine the influence of the individual bond parameters. Apparently, compressive stresses on the plate reinforcement and a good roughening of the concrete surface prior to the application of the plates provide an enhanced bond strength.

The shear failure of concrete structures is often dominated by a mechanism which corresponds to the inclined crack opening process. Hence, the *MICO* has the potential to be used as an analysis tool for such cases.

REFERENCES

1. Meier, U., Deuring, M., Meier, H., Schwegler, G.: *Strengthening of structures with advanced composites*. Alternative materials for the reinforcement and prestressing of concrete, Blackie academic & professional, Chapman & Hall, Glasgow, UK, 1993, pp. 153-171.

2. Holzenkämpfer, P.: *Ingenieurmodelle des Verbunds geklebter Bewehrung für Betonbauteile (Bond Models for Externally Bonded Reinforcement for Concrete Structures)*. Deutscher Ausschuss für Stahlbeton, Heft 473, Berlin, Germany, 1997, pp. 109-209.

3. Ulaga, T.: *Betonbauteile mit Stab- und Lamellenbewehrung: Verbund- und Zuggliedmodellierung (Concrete members with Internal Bar and External Plate Reinforcement: Bond and Tension Chord Modelling)*. Dissertation ETH 15062 (PhD thesis), ETH Zürich, Switzerland, March 2003, 161 pp.

4. Neubauer, U.: *Verbundverhalten geklebter Lamellen aus Kohlenstoff-Verbundwerkstoffen zur Verstärkung von Betonbauteilen (Bond Behaviour of CFRP Laminates for the Strengthening of Concrete Structures)*. Dissertation, Institut für Baustoffe, Massivbau und Brandschutz, TU Braunschweig, Heft 150, Braunschweig, Germany, 2000, 242 pp.

5. Ranisch, E.-H.: *Zur Tragfähigkeit von Verklebungen zwischen Baustahl und Beton – Geklebte Bewehrung (The Anchorage Capacity of Plate Reinforcement on Concrete Structures)*. Dissertation, Institut für Baustoffe, Massivbau und Brandschutz, TU Braunschweig, Heft 54, Braunschweig, Germany, 1982, 173 pp.

6. Täljsten, B.: *Plate Bonding. Strengthening of Existing Concrete Structures with Epoxy Bonded Steel or Fibre Reinforced Plastics*. Doctoral thesis, Division of Structural Engineering, Lulea University, Sweden, 1994, 190 pp.

7. Neubauer, U., Rostásy, F.S.: *Bond Failure of Fiber Reinforced Polymer Plates at Inclined Cracks – Experiments and Fracture Mechanics Model*. Proceedings of the FRPRCS-4 Symposium, Baltimore, USA, 1999, pp. 369-381.

8. Ulaga, T., Vogel, T., Meier, U.: *The Bilinear Stress-Slip Bond Model: Theoretical Background and Significance*. Proceedings of the FRPRCS-6 Symposium, Singapore, 2003, pp. $$$-$$$.

9. Marti, P., Alvarez, M., Kaufmann, W., Sigrist, V.: *Tragverhalten von Stahlbeton* (*The Behaviour of Structural Concrete*). Institut für Baustatik und Konstruktion, ETH Zürich, IBK Publikation SP-008, Zürich, Switzerland, 1999, 301 pp.

10. Walraven, J. C.: *Aggregate Interlock: A Theoretical and Experimental Analysis*. PhD thesis, Delft University of Technology, Delft University Press, 1980, 197 pp.

11. Walraven, J. C., Reinhard, H.W.: *Theory and Experiments on the Mechanical Behaviour of Cracks in Plain and Reinforce Concrete Subjected to Shear Loading*. Heron, Vol. 26, no. 1A, 1981, pp. 1…68.

12. Keller, T.: *Dauerhaftigkeit von Stahlbetontragwerken (The Durability of Concrete Structures)*. Institut für Baustatik und Konstruktion, ETH Zürich, IBK Bericht Nr. 184, Switzerland, 1991, 206 pp.

13. CEB: *CEB-FIP Model Code 1990*. Comité Euro-International du Béton, Published by Thomas Telford, London, 1993, 437 pp.

14. Ulaga, T., Meier, U.: *Kohlenstofffaserverstärkte thermoplastische Lamellen für die Verstärkung von Betontragwerken (Carbon Fibre Reinforced Thermoplastic Laminates for the Strengthening of Concrete Structures)*. EMPA Bericht Nr. 260, Zürich, Switzerland, 2002, 112 pp.

LIST OF FIGURES

FIGURES

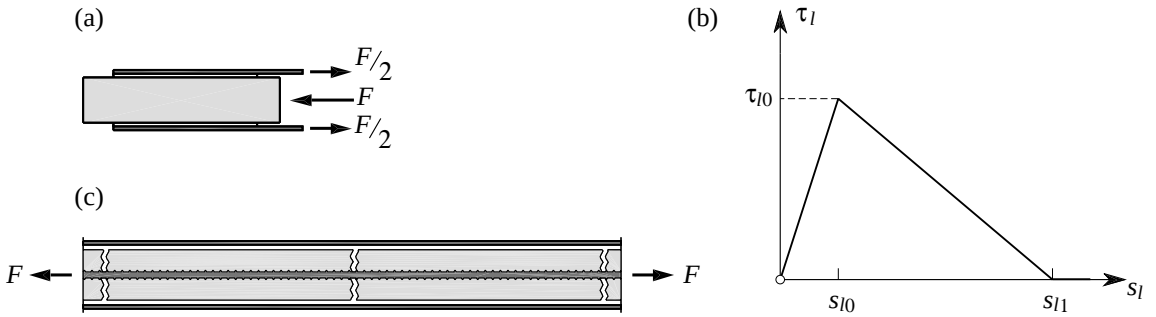

Fig. 1—The bilinear bond stress-slip relationship: (a) analysis of the anchorage capacity; (b) diagram; (c) analysis of a tension chord with mixed reinforcement.

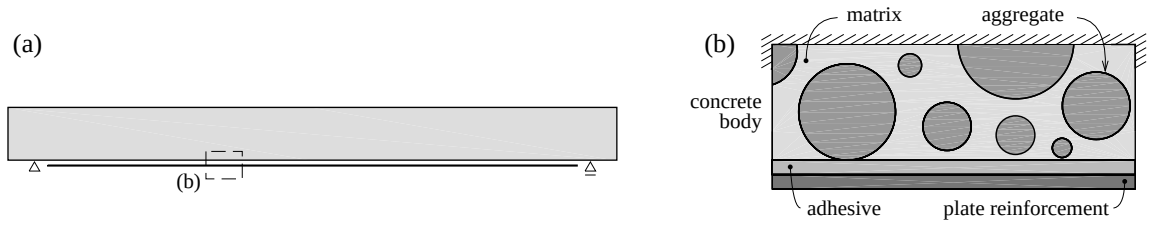

Fig. 2—Unloaded concrete structure with plate reinforcement: (a) overview; (b) detail.

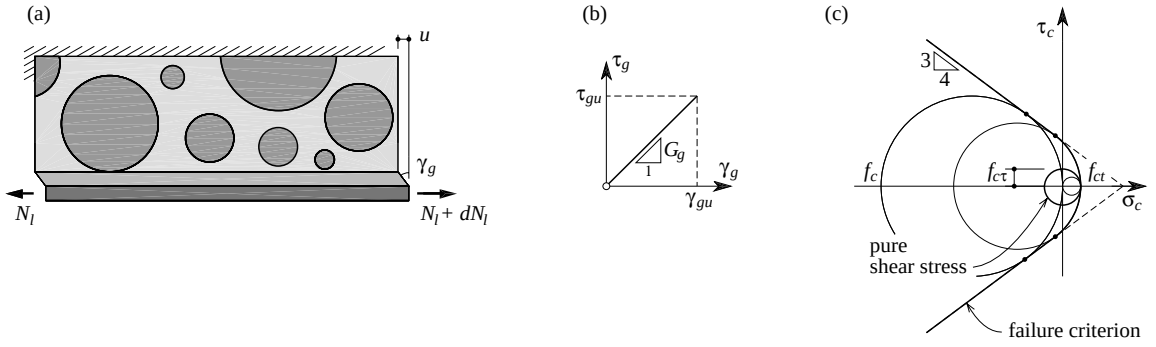

Fig. 3—"Bond at low load": (a) detail; (b) shear stress-shear strain diagram of the adhesive layer; (c) modified Coulomb failure criterion.

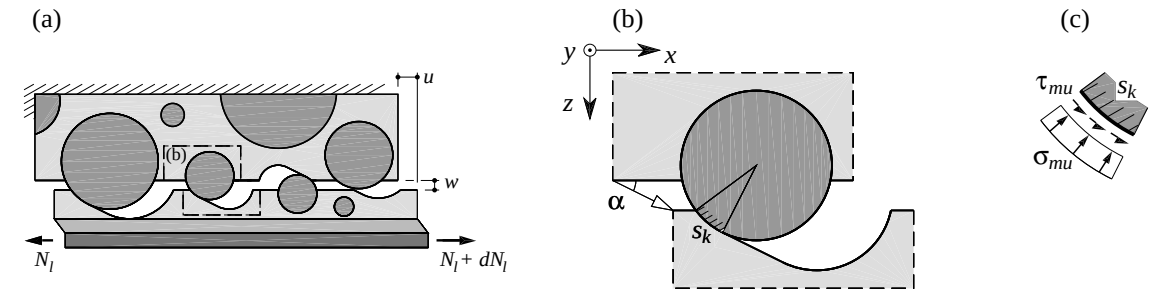

Fig. 4—"Bond at high load": (a) detail; (b) single aggregate particle; (c) contact stresses.

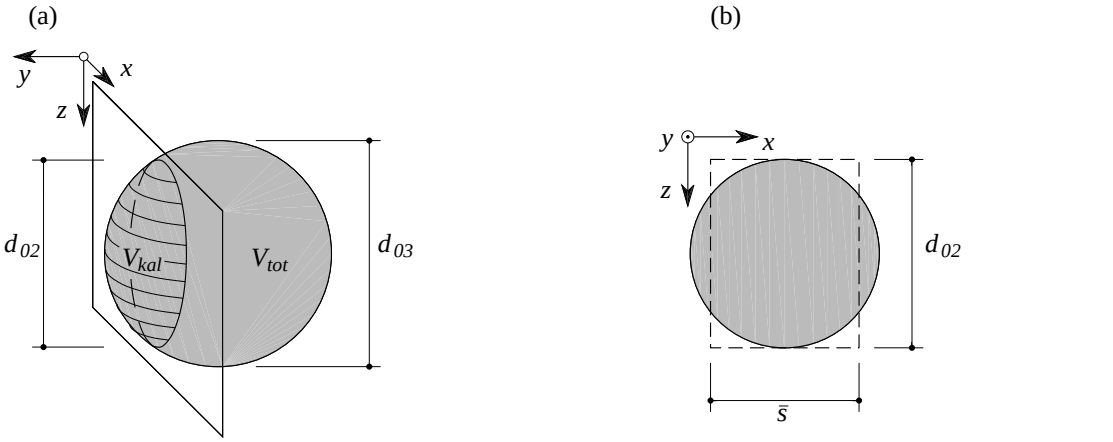

Fig. 5—Single aggregate particle: (a) intersection circle; (b) average length of a secant.

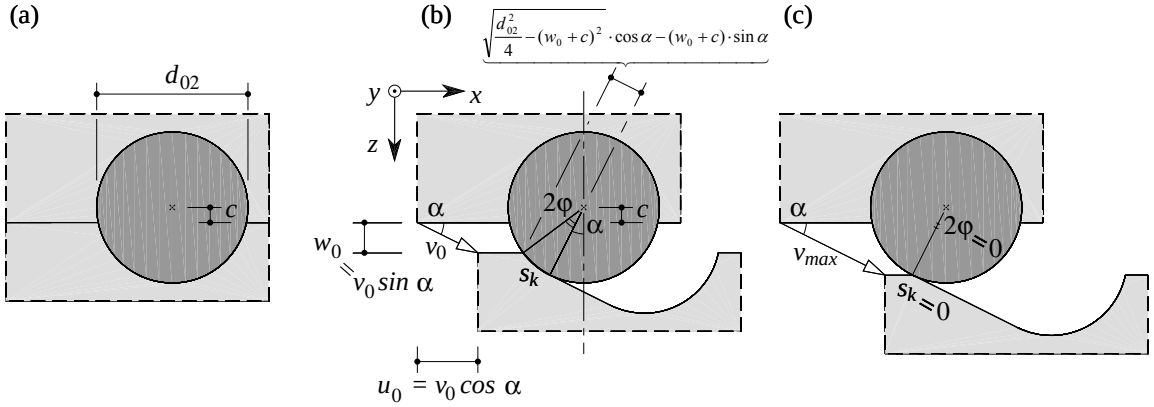

Fig. 6—Crack opening: (a) crack is closed; (b) general case; (c) contact disappears.

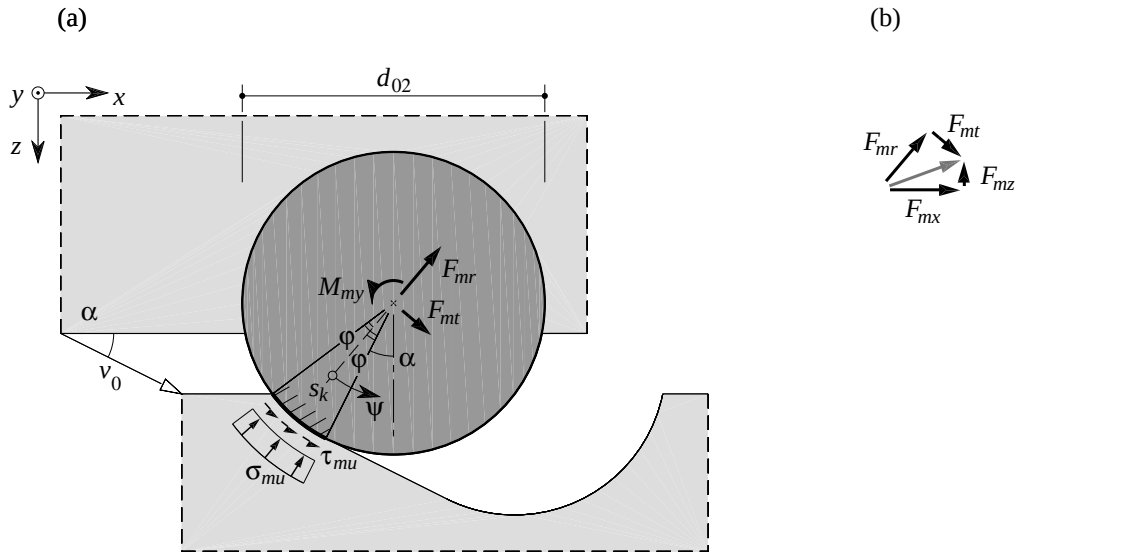

Fig. 7—Single aggregate particle: (a) resulting contact forces; (b) components of the contact force.

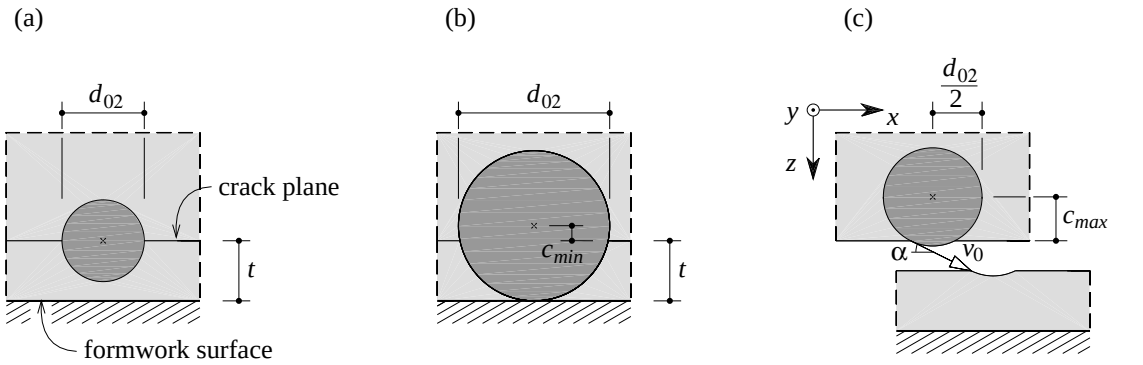

Fig. 8—Boundary conditions: (a) "small" aggregate particle; (b) "big" aggregate particle; (c) "large" embedment depth.

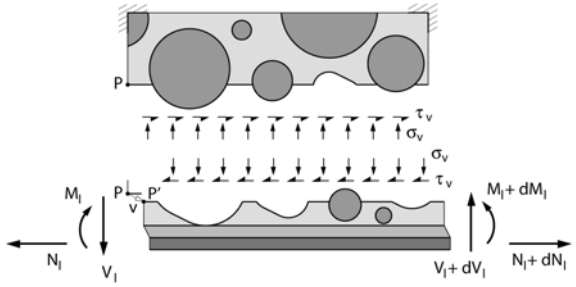

Fig. 9—Inclined crack opening: interlocking stresses.

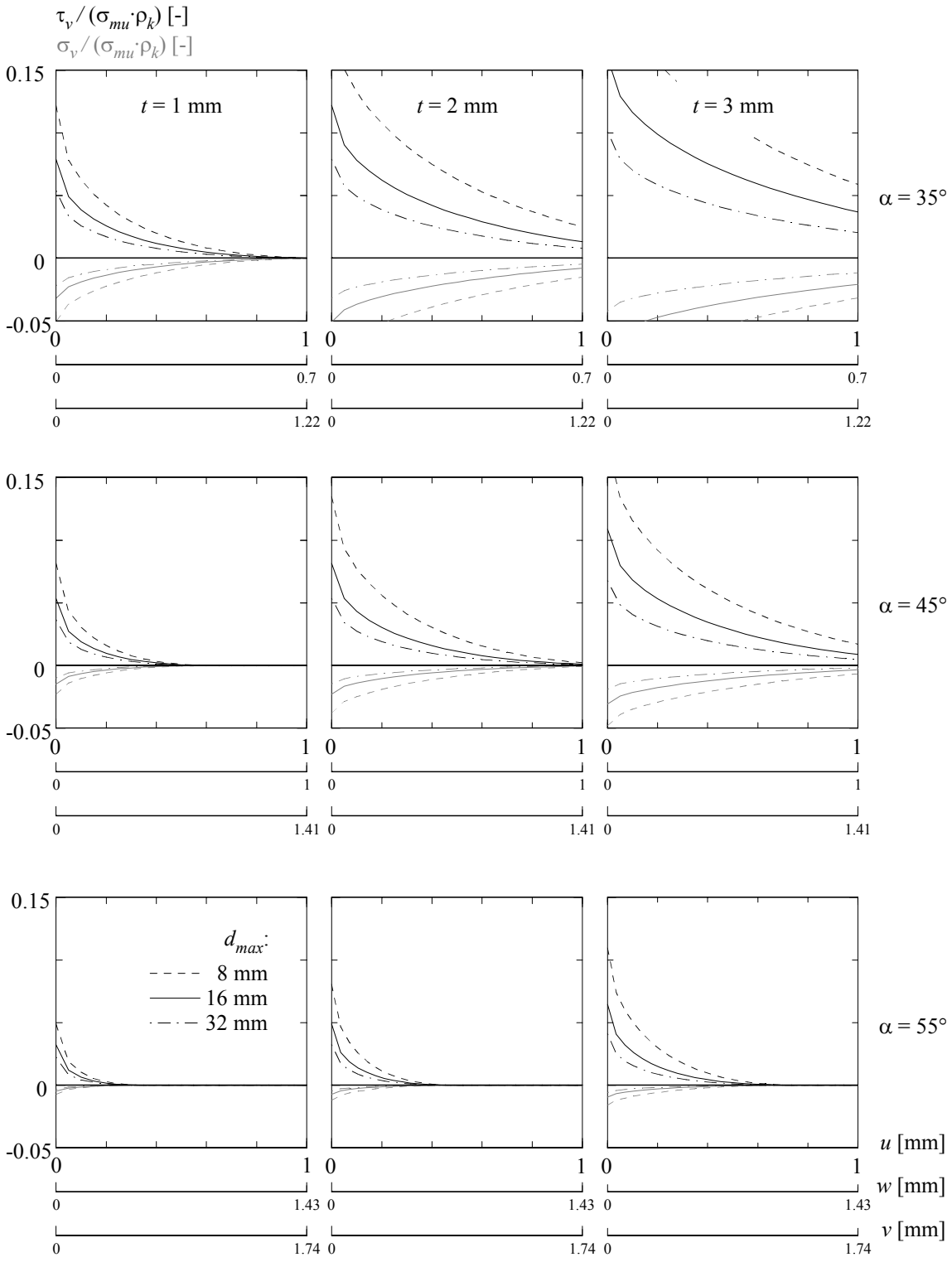

Fig. 10—Evaluation of the MICO: interlocking stresses for varying values of the parameters α, t and d_{max}.

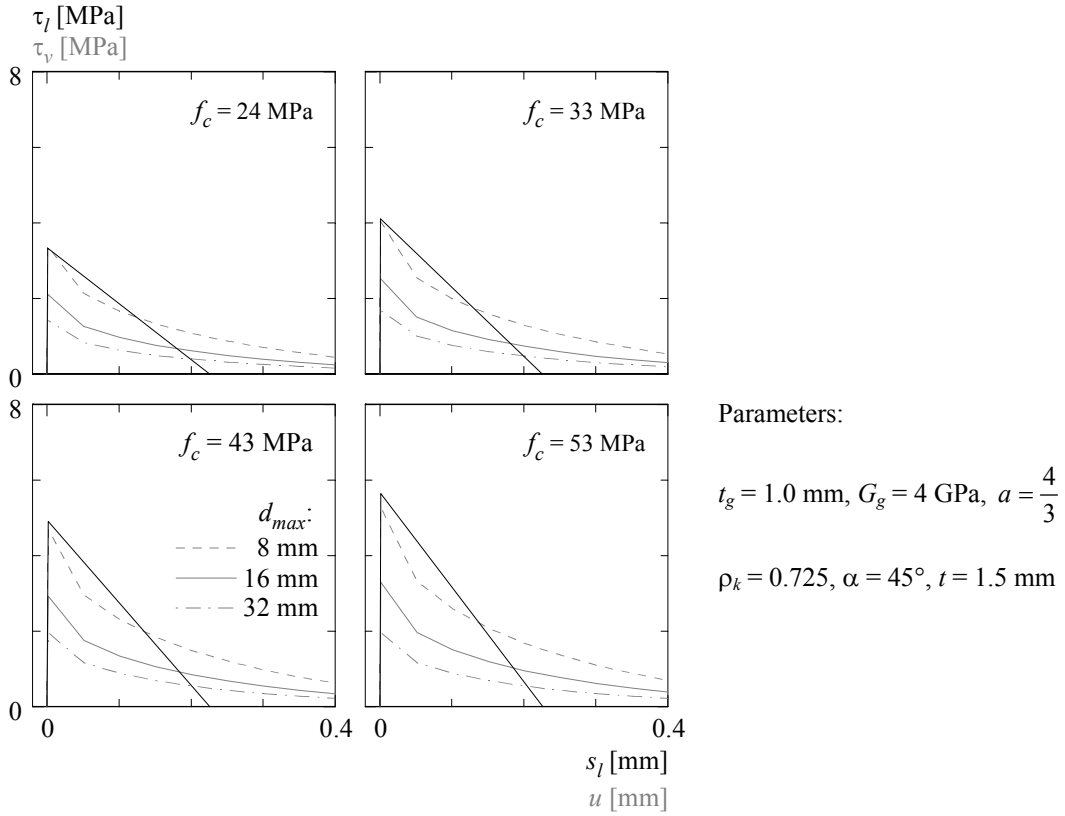

Fig. 11—"Bond at low load", "bond at high load" and the bilinear bond stress-slip relationship.

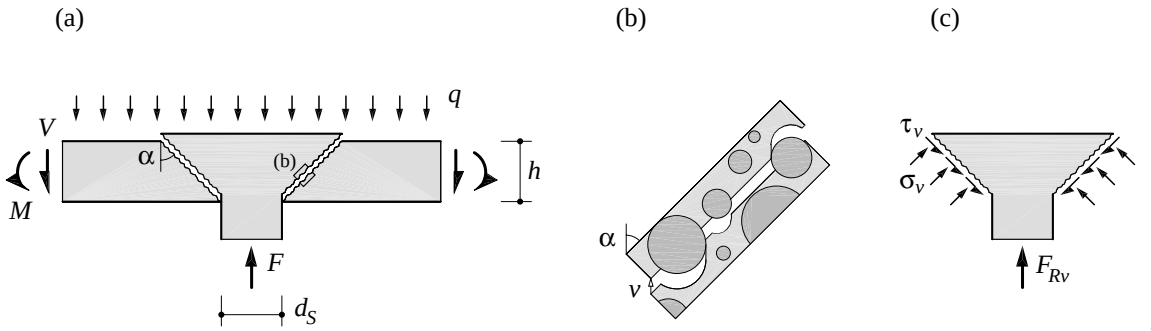

Fig. 12—Punching of a flat slab: (a) overview; (b) detail; (c) interlocking stresses.

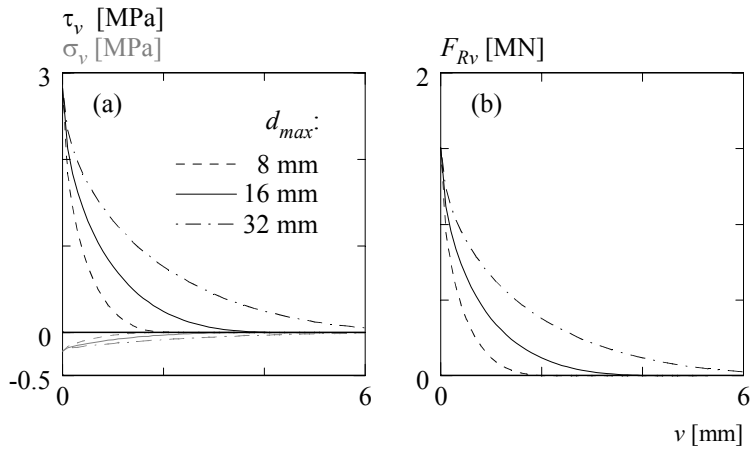

Parameters:

f_c = 24 MPa (σ_{mu} = 42.9 MPa)

ρ_k = 0.725

α = 60°

d_s = 400 mm, h = 240 mm

Fig. 13—Punching of a flat slab: numerical example.